Supporting Information

Kubota *et al.* 10.1073/pnas.0804055106

SI Materials and Methods

Plasmids and Germline Transformation. WT *let-2* was amplified by PCR from the cosmid clone F01G12 and cloned into a modified Fire vector pKOGzerob (1). This construct contains a 3.8-kb 5′-noncoding region, the entire coding region and the 3′-noncoding region corresponding to nucleotide positions 10147–22830 of the cosmid F01G12. *let-2(k193)* and *let-2(k196)* genes were constructed by introducing the *k193* and *k196* mutations, respectively, into the WT construct. The *nid-1* gene corresponding to nucleotide positions 497–10095 of the cosmid F54F3, which includes a 2.0-kb promoter, the entire coding region and 3′-noncoding region, was cloned into a modified pBluescript II KS(-) vector. The HA (YPYDVPDYA) coding sequence was introduced immediately after the *nid-1* coding region. Germline transformation was performed by injecting DNA mixture into the gonad (2). WT and mutant *let-2* plasmids were injected at 6 ng/μl with 124 ng/μl carrier DNA, pBluescript II KS(-) and 20 ng/μl *unc-119*$^{+}$ plasmid (pDP#MM016B) (3). *nid-1*::*HA* was injected at 5 ng/μl with 65 ng/μl pBluescript II KS(-), 10 ng/μl *unc-119*$^{+}$ plasmid and 70 ng/μl marker plasmid, *sur-5*::*GFP*. Higher concentrations of *let-2* and *nid-1* plasmids were toxic.

1. Ohkura K, *et al.* (2003) SDF-9, a protein tyrosine phosphatase-like molecule, regulates the L3/dauer developmental decision through hormonal signaling in *C. elegans*. *Development* 130:3237–3248.
2. Mello CC, *et al.* (1991) Efficient gene transfer in *C. elegans*: Extrachromosomal maintenance and integration of transforming sequences. *EMBO J* 10:3959–3970.
3. Maduro M, Pilgrim D, (1995) Identification and cloning of *unc-119*, a gene expressed in the *Caenorhabditis elegans* nervous system. *Genetics* 141:977–988.
4. Wicks SR, *et al.* (2001) Rapid gene mapping in *Caenorhabditis elegans* using a high density polymorphism map. *Nat Genet* 28: 160–164.
5. Kubota Y, Kuroki R, Nishiwaki K (2004) A fibulin-1 homolog interacts with an ADAM protease that controls cell migration in *C. elegans*. *Curr Biol* 14:2011–2018.
6. Hesselson D, Kimble J, (2006) Growth control by EGF repeats of the *C. elegans* Fibulin-1C isoform. *J Cell Biol* 175: 217–223.
7. Merz DC, *et al.* (2003) UNC-52/perlecan affects gonadal leader cell migrations in *C. elegans* hermaphrodites through alterations in growth factor signaling. *Dev Biol* 256:173–186.
8. Ackley BD, *et al.* (2001) The NC1/endostatin domain of *Caenorhabditis elegans* type XVIII collagen affects cell migration and axon guidance. *J Cell Biol* 152:1219–1232.
9. Forrester WC, Garriga G, (1997) Genes necessary for *C. elegans* cell and growth cone migrations. *Development* 124:1831–1843.

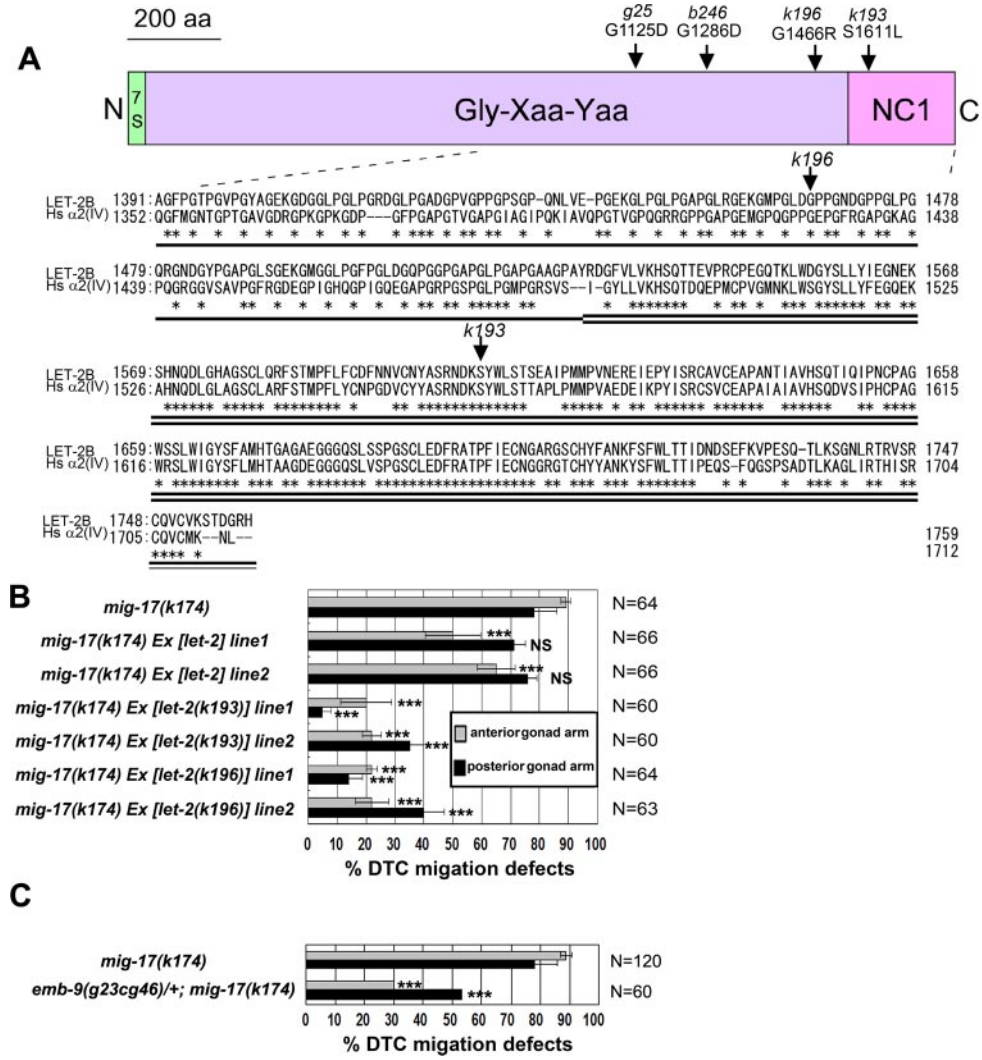

Fig. S1. Molecular cloning of *let-2* and transgenic rescue experiments.(*A*) (*Upper*) Domain structure of LET-2 and locations of mutations used in this study. Amino acid substitutions are shown. Amino acid numbers of LET-2 correspond to those of LET-2B. The *k193* mutation is a TCA-to-TTA transition, resulting in a Ser-to-Leu substitution at position 1610 in the LET-2A NC1 domain and a Ser-to-Leu substitution at position 1611 in the LET-2B NC1 domain. The *k196* mutation is a GGA-to-AGA transition that changes the conserved Gly-1465 to Arg in LET-2A and Gly-1466 to Arg in LET-2B. N, amino terminus, C, carboxyl terminus. (*Lower*) Alignment of the C-terminal sequences of type IV collagen α2 chains of *C. elegans* (LET-2) and human (Hs α2 (IV)). Part of the Gly-X-Y domain is underlined. Double underlines indicate the NC1 domain. Identical amino acids are indicated by asterisks. The sites of the suppressor mutations are indicated. The suppressor mutants, *k193* and *k196*, were isolated as described (5) and were mapped to the linkage group X. The *unc-7(e139) let-2(k196); mig-17(k174)* triple mutant were crossed with *mig-17(k174)* animals, which were outcrossed ten times to CB4856, a strain for single nucleotide polymorphism (SNP) mapping (4). The analysis of SNPs in the recombinants revealed that the *k196* mutation is ≈100 kb to the right of a SNP in the cosmid region ZK1073. A search of the WormBase for ECM protein genes in this region identified *let-2* (*F01G12.5*), which encodes the α2 chain of type IV collagen. The PCR amplification product of *let-2* from *mig-17(k174); let-2(k196)* rescued the DTC migration defects of *mig-17(k174)* mutants. Missense mutations were found in *let-2* in both the *k196* and *k193* mutants by DNA sequence analysis. (*B*) Effects of WT and mutant *let-2* transgenes on *mig-17* suppression. Percentages of animals with anterior and posterior DTC migration defects are shown. Error bars represent the mean SD. (*C*) Effect of *emb-9* gene dosage on *mig-17* defects. *unc-36(e251)emb-9(g23cg46)/hT2[gIs48]; mig-17(k174)* males were mated with *unc-42(e270) mig-17(k174)* hermaphrodites, and GFP-negative and non-uncoordinated movement cross-progeny were scored. Results for Fisher's exact test against *mig-17(k174)* are indicated: ***, $P < 0.001$; NS, not significant.

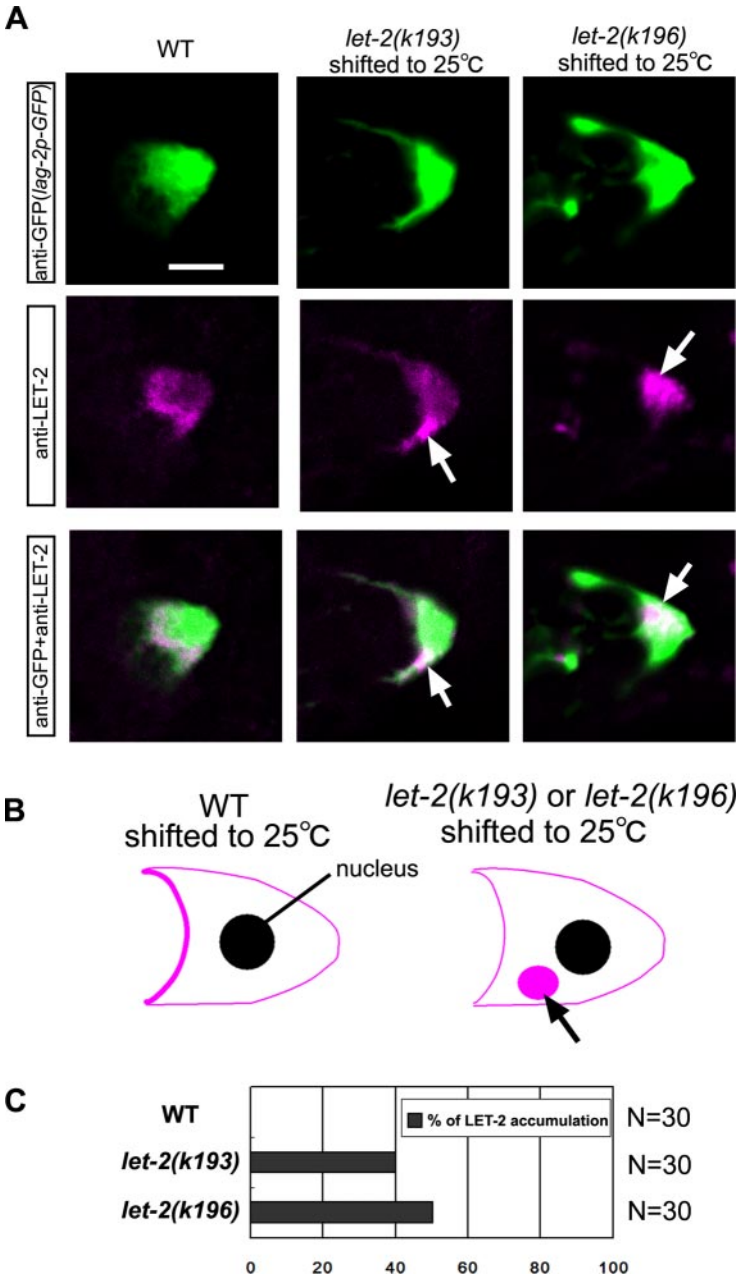

Fig. S2. LET-2 expression in DTCs. (*A*) LET-2 expression in DTCs. Animals were shifted to 25 °C at L2 stage and sectioned at L4 stage. Frozen sections of WT (*Left*), *let-2(k193)* (*Center*) and *let-2(k196)* (*Right*) animals with integrated *lag-2*::*GFP,* which is expressed in DTCs, are shown. Sections were stained with anti-GFP (*Upper*, green), anti-LET-2 (*Middle*, magenta). Merged images are shown (*Lower*). Arrows indicate cytoplasmic accumulation of mutant LET-2 proteins. The intense anti-LET-2 staining in the WT section corresponds to LET-2 localization to the BM between the DTC and the germline. (Scale bar, 5 μm.) (*B*) Schematic representation of LET-2 localization to DTCs. Localization of LET-2 proteins to the surface or cytoplasm of DTCs is shown in magenta. (*C*) Percent cytoplasmic accumulation of LET-2 in DTCs. $n = 30$. Both LET-2(*k193*) and LET-2(*k196*) localized to the pharyngeal BM at 20 °C and 25 °C (data not shown).

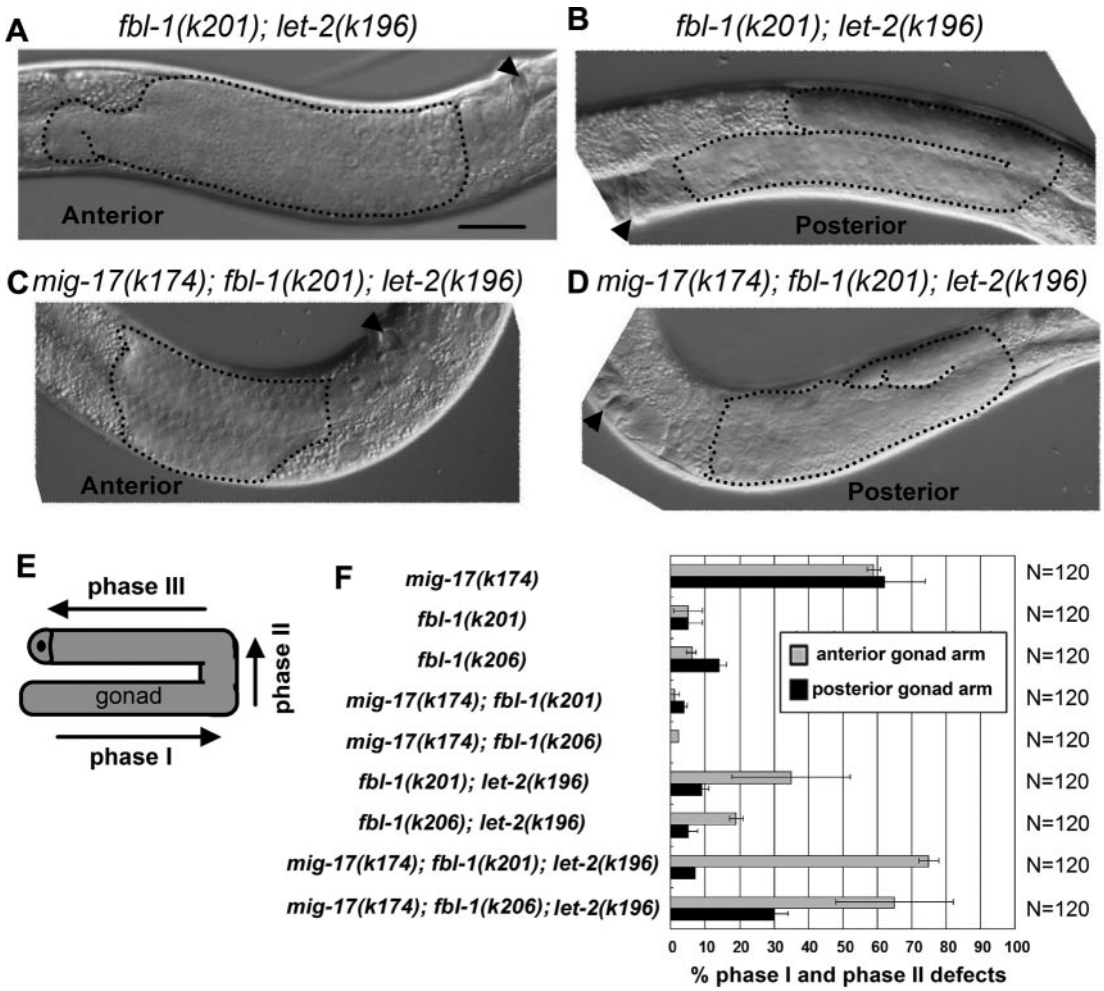

Fig. S3. Synergistic effect of *let-2* and *fbl-1* on gonad formation. (*A-D*) Stippled lines indicate the gonads. Arrowheads indicate the vulvae. Phenotypes of anterior (*A*, *C*) and posterior (*B*, *D*) gonads of *fbl-1(K201); let-2(k196)* (*A*, *B*) and *mig-17(k174); fbl-1(K201); let-2(k196)* (*C*, *D*) animals are shown. (Scale bar, 50 μm.) (*E*) Migration phases of the DTC. (*F*) Quantification of phase I and phase II defects. Error bars represent the mean SD. Although migration of the posterior DTCs in the triple mutants stopped before reaching the vulva, the posterior arms formed a U shape more often than they did in *mig-17(k174)* mutants, indicating that the migration defects of posterior DTCs in *mig-17* are suppressed in the *fbl-1; let-2* double mutant backgrounds. *fbl-1; let-2(k196)* and *mig-17(k174); fbl-1; let-2(k196)* animals lacking a GFP signal were segregated from *fbl-1/nT1[qIs51]IV; +/nT1[qIs51]V; let-2(k196)* and *fbl-1/nT1[qIs51] IV; mig-17(k174)/nT1[qIs51] V; let-2(k196)*, respectively. Although a defect in organism growth has been reported in the *fbl-1(tk45)* null mutant (6), such a defect was not detected in *fbl-1(k201); let-2(k196)* double mutants (data not shown).

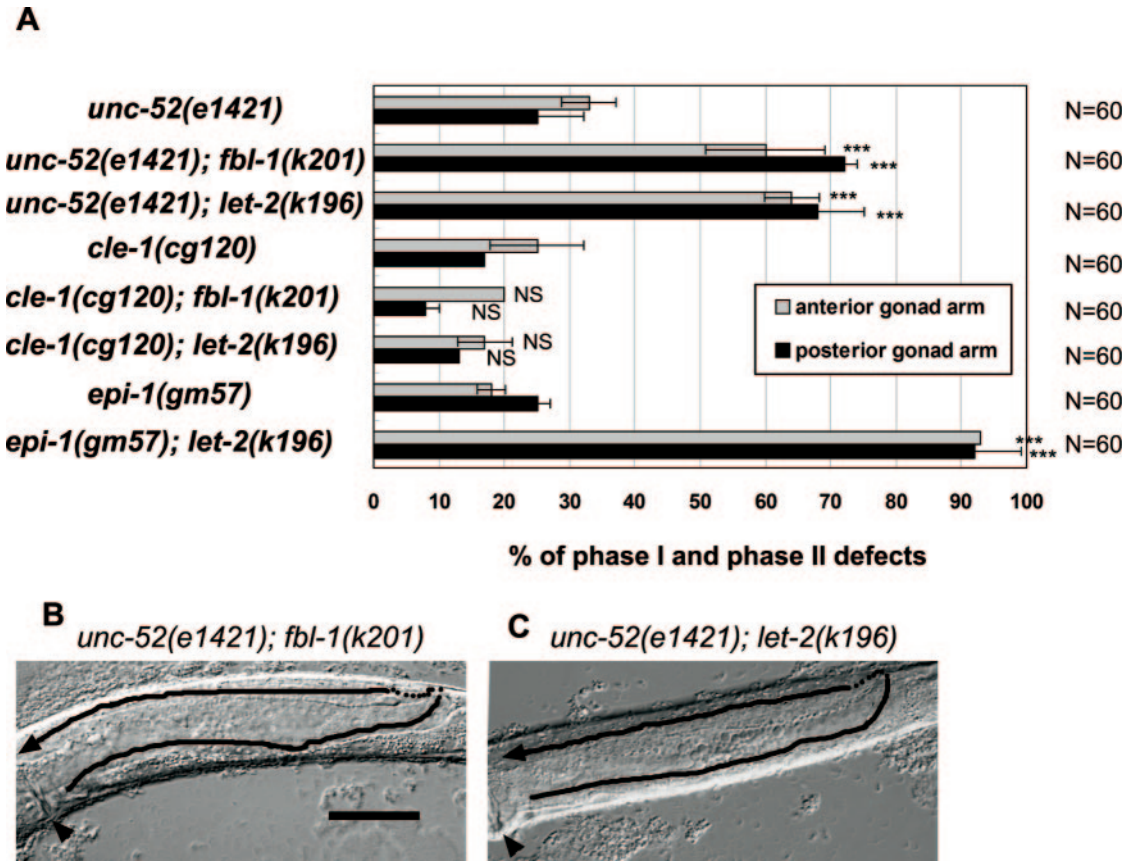

Fig. S4. Synergistic effects of *unc-52, epi-1, let-2* and *fbl-1* on gonad formation. (*A*) Quantification of phase I and phase II defects in *unc-52, cle-1* and *epi-1* individual mutants and in those combined with *fbl-1* and *let-2*. Error bars represent the mean SD. Fisher's exact test was performed between single and double mutants: ***, $P < 0.001$; NS, not significant. *unc-52*(*e1421*), *cle-1*(*cg120*), and *epi-1*(*gm57*) having DTC migration defects were used in this analysis (7, 8, 9). *unc-52*(*e1421*) and *cle-1*(*cg120*) showed precocious dorsal migration. *epi-1*(*gm57*) showed variable migration defects. (*B*, *C*) Precocious dorsal migration in *unc-52* and *fbl-1* or *let-2* double mutants. (Scale bar, 50 μm.)

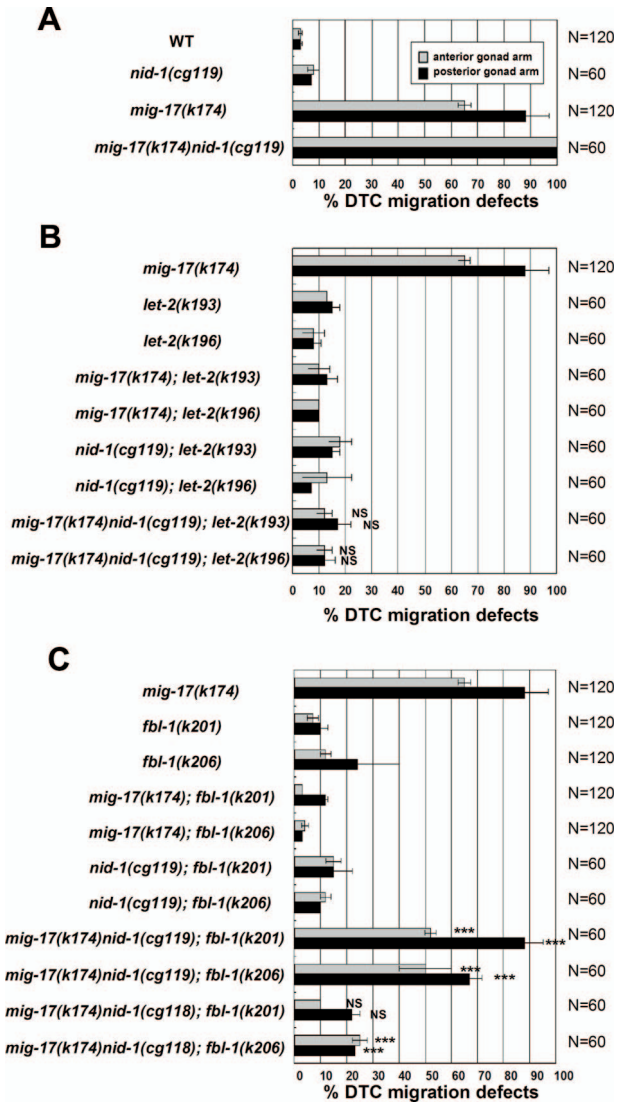

Fig. S5. NID-1-dependence of suppression. (*A*-*C*) Quantification of directional DTC migration defects of *nid-1*, *mig-17* and the double mutants (*A*), *let-2*-containing strains (*B*), and *fbl-1*-containing strains (*C*). Error bars represent the mean SD. In (*B*) Fisher's exact test was performed between *mig-17; let-2* double and *mig-17nid-1; let-2* triple mutants. In (*C*) Fisher's exact test was performed between *fbl-1; mig-17* double and *fbl-1; mig-17nid-1* triple mutants. ***, $P < 0.001$; NS, not significant.

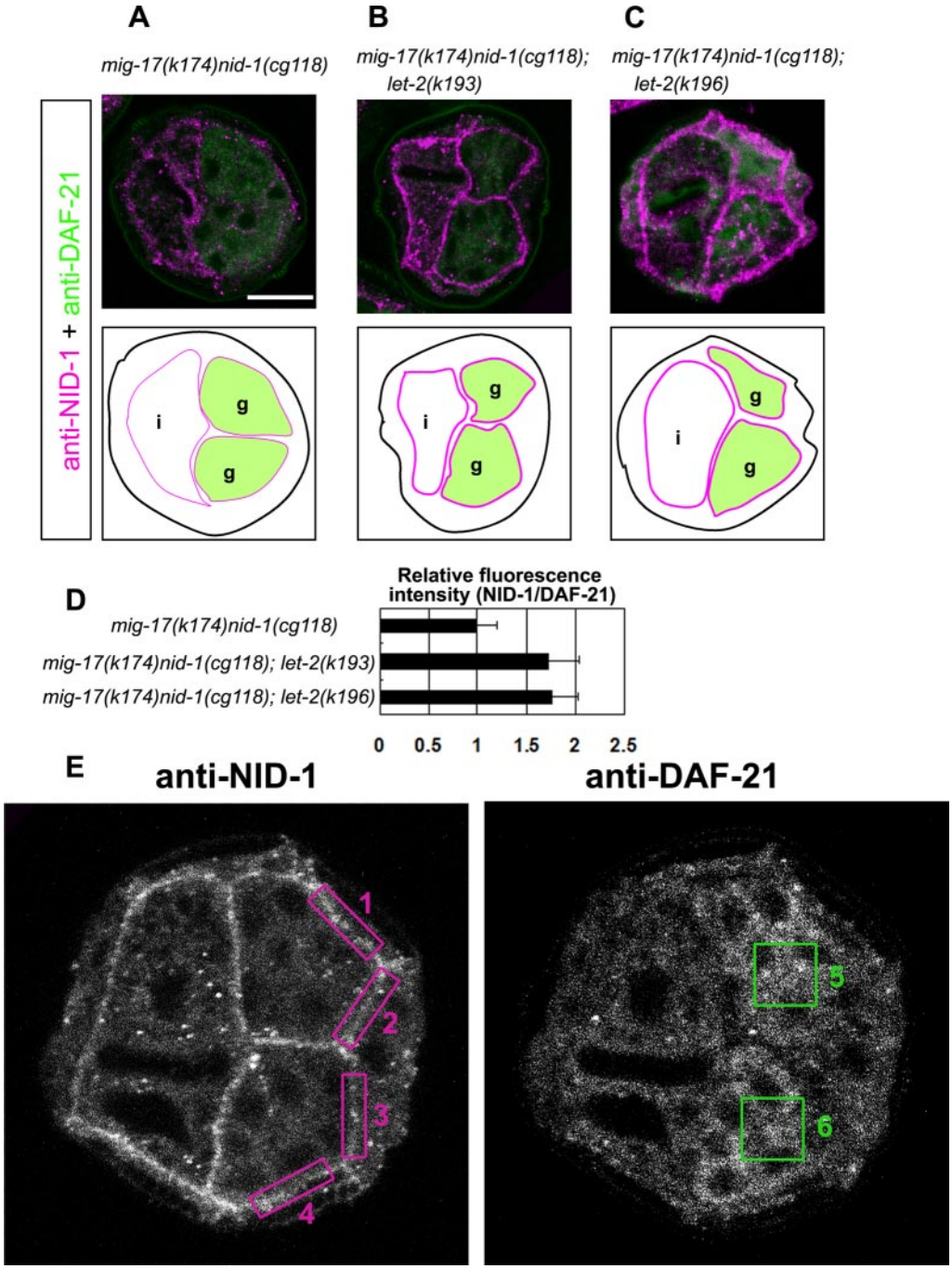

Fig. S6. Suppressor *let-2* mutations recruit NID-1 lacking the G2 domain. Cross-sections of L4 hermaphrodites were stained with anti-NID-1 (magenta), anti-DAF-21(green). Localization of NID-1 in *mig-17(k174) nid-1(cg118)* (*A*), *mig-17(k174) nid-1(cg118); let-2(k193)* (*B*) and *17(k174) nid-1(cg118); let-2(k196)* (*C*). Borders of gonads and intestines are illustrated below the photos. Levels of NID-1 localization to the BM are indicated by magenta thick lines (normal levels) and thin lines (low levels). g, gonad; i, intestine. (Scale bar, 12.5 μm.) (*D*) Fluorescence intensity of anti-NID-1 relative to that of anti-DAF-21. The relative fluorescence intensity for each sample was normalized by that of *mig-17 nid-1(cg118)*. Confocal images of three well-stained sections were selected from each strain and used for quantification. (*E*) Method for quantification of fluorescence. Sample images of a section co-stained with anti-NID-1 and anti-DAF-21 are shown. For anti-NID-1 quantification, four areas [1 to 4, indicated by magenta rectangles (2 μm $\times$ 8 μm)] were chosen to represent the dorsal surface of the distal gonad, the lateral surface of the distal gonad, the lateral surface of the proximal gonad, and the ventral surface of the proximal gonad, respectively, and the fluorescence intensity of each area was quantified using the ImageJ program (National Institutes of Health) and the average intensity was calculated ($n = 3$). For anti-DAF-21 quantification, two areas [5 and 6, indicated by green squares (6 μm $\times$ 6 μm)] were chosen that represent the center of the distal and proximal gland, respectively, and were analyzed similarly.

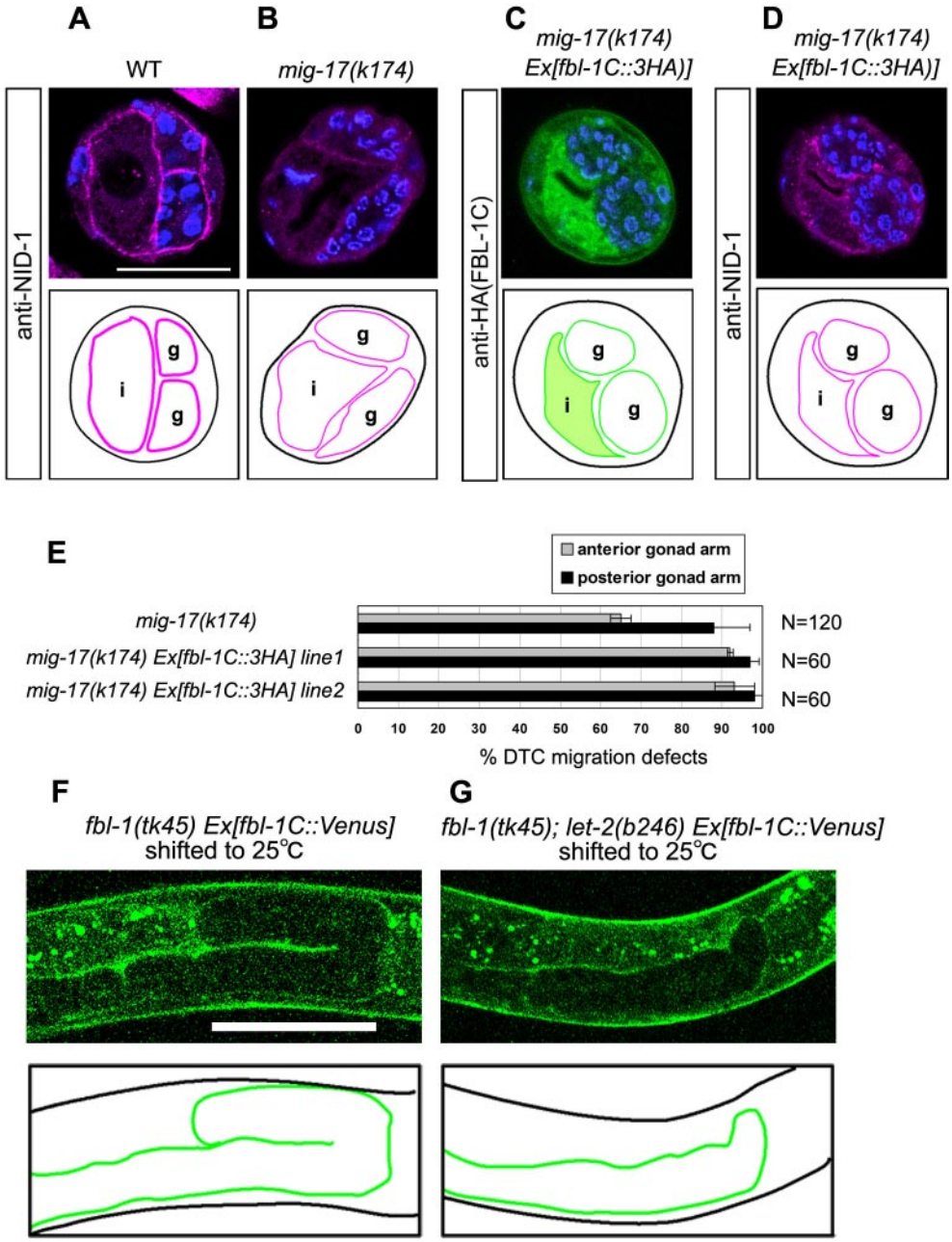

Fig. S7. Effects of FBL-1C-3HA overexpression and LET-2 reduction. (*A-D*) Cross-sections of L4 hermaphrodites were stained with anti-NID-1 (magenta), anti-HA (green), and DAPI (blue). Localization of NID-1 in WT (*A*), *mig-17(k174)* (*B*) and *mig-17(k174) Ex [fbl-1C::3HA]* (*D*) animals. (*C*) Localization of FBL-1C-3HA (green) in *mig-17(k174) Ex[fbl-1C::3HA].* The same section as in (*D*) was stained with anti-HA. FBL-1C-3HA is highly expressed in the intestine. Borders of gonads and intestines are illustrated below the photos. Levels of NID-1 localization to the BM are indicated by magenta thick lines (normal levels) and thin lines (low levels). FBL-1C-3HA localization to the BM is indicated by green lines. g, gonad; i, intestine. (*E*) Quantification of DTC migration defects of *mig-17* and *mig-17 Ex[fbl-1C::3HA]*. Overexpression of FBL-1C exacerbates defective DTC migration in *mig-17*. Error bars represent the mean SD. (*F*, *G*) Localization of FBL-1C-Venus in *fbl-1(tk45) Ex[fbl-1C::Venus]* (*F*) and in *fbl-1(tk45); let-2(b246) Ex[fbl-1C::Venus]* (*G*) animals. Animals were shifted to 25 °C at L2 stage and examined by confocal microscopy at L4 stage. FBL-1C-Venus localization to the gonadal BM is indicated by green lines. (Scale bars, 25 μm.) FBL-1C-Venus localized normally in both *let-2(+)* and *let-2(b246)*, suggesting that FBL-1C is not involved in the recruitment of NID-1 by LET-2.

Table S1. Lethality of *let-2* mutants

Assay temp.	16 °C				20 °C				25 °C			
Strain	E	L	A	N	E	L	A	N	E	L	A	N
Wild type	0	0	100	191	0	0	100	223	0	0	100	322
let-2(g25)	0	0	100	178	0	0	100	229	96	4	0	296
let-2(k193)	16	0	84	110	13	1	87	152	20	1	79	192
let-2(k196)	0	0	100	128	0	0	100	159	7	85	8	131

E: percentage of embryonic lethality; L: percentage of larval lethality: A: percentage of animals that grown to the adult stage; N: numbers of animals scored.

Table S2. Gonad phenotype of various *let-2* mutants in wild-type and *mig-17* mutant backgrounds

Strain	A, %	P, %	N
Wild type	0	0	75
mig-17(k174)	87	82	60
let-2(g25)	2	2	60
let-2(b246)	7	5	60
mig-17(k174); let-2(g25)	73*	62**	60
mig-17(k174); let-2(b246)	68***	70^{NS}	60

Experiments were conducted at 20 °C. A: misshapen anterior gonad arms; P: misshapen posterior gonad arms; N: number of animals scored. Fisher's exact tests were performed between *mig-17(k174)* single and *mig-17(k174); let-2* double mutants. **, $P < 0.05$; **, $P < 0.01$; ***, $P < 0.001$*; NS, not significant.

Table S3. Suppression of *mig-17* by canonical *let-2* mutations in temperature

Shifted stage	L2			L3		
Strain	A	P	N	A	P	N
Wild type	0	0	53	0	0	15
mig-17(k174)	95	93	75	99	91	15
let-2(g25)	0	0	34	ND	ND	ND
let-2(b246)	0	0	20	0	0	20
mig-17(k174); let-2(g25)	87^{NS}	25***	60	78^{NS}	68***	60
mig-17(k174); let-2(b246)	73***	43***	30	87^{NS}	70***	30

Cultivation temperature was shifted from 20 °C to 22.5 °C at the indicated stages. A: percentage of misshapen anterior gonad arms; P: percentage of misshapen posterior gonad arms; N: number of animals scored. ND: not determined; Fisher's exact test were performed between *mig-17(k174)* single and *mig-17(k174); let-2* double mutants. ***, $P < 0.001$; NS, not significant.